

AUTHOR QUERY FORM

 ELSEVIER	Journal: YJSVI Article Number: 9942	Please e-mail or fax your responses and any corrections to: E-mail: corrections.eseo@elsevier.macipd.com Fax: +44 1392 285878
--	--	--

Dear Author,

Any queries or remarks that have arisen during the processing of your manuscript are listed below and highlighted by flags in the proof. Please check your proof carefully and mark all corrections at the appropriate place in the proof (e.g., by using on-screen annotation in the PDF file) or compile them in a separate list.

For correction or revision of any artwork, please consult <http://www.elsevier.com/artworkinstructions>.

Articles in Special Issues: Please ensure that the words ‘this issue’ are added (in the list and text) to any references to other articles in this Special Issue

Uncited references: References that occur in the reference list but not in the text – please position each reference in the text or delete it from the list.	
Missing references: References listed below were noted in the text but are missing from the reference list – please make the list complete or remove the references from the text.	
Location in article	Query/remark Please insert your reply or correction at the corresponding line in the proof
	No queries

Electronic file usage

Sometimes we are unable to process the electronic file of your article and/or artwork. If this is the case, we have proceeded by:

- Scanning (parts of) your article
 Rekeying (parts of) your article
 Scanning the artwork

Thank you for your assistance.



Contents lists available at ScienceDirect

Journal of Sound and Vibration

journal homepage: www.elsevier.com/locate/jsv

Scattering of flexural wave in a thin plate with multiple circular inclusions by using the null-field integral equation approach

W.M. Lee^a, J.T. Chen^{b,*}^a Department of Mechanical Engineering, China University of Science and Technology, Taipei, Taiwan^b Department of Harbor and River Engineering, National Taiwan Ocean University, P.O. Box 7-59, Keelung 20224, Taiwan

ARTICLE INFO

Article history:

Received 17 March 2009

Received in revised form

11 August 2009

Accepted 11 October 2009

Handling Editor: L.G. Tham

ABSTRACT

The subject of scattering flexural wave in a thin plate with multiple circular inclusions under the incident flexural wave is studied in this paper. A semi-analytical approach is proposed to solve this problem which can be decomposed into several interior circular inclusion problems and an exterior plate problem subject to the incident wave. The scattered field in the associated exterior problem is solved by using the null-field integral formulation in conjunction with degenerate kernels, tensor transformation and Fourier series. All dynamic kernels of plate in the direct formulation are expanded into degenerate forms to avoid the integral singularity and further the rotated degenerate kernels have been derived to consider the general case of multiple circular inclusions. The proposed results for an infinite plate with one circular inclusion are compared with the available analytical solutions to verify the validity of the proposed method. To demonstrate the generality of the proposed method, the cases of multiple inclusions are studied and their quasi-static results are verified by static data of FEM using ABAQUS. Numerical results indicate that the DMCF of two inclusions is apparently larger than that of one when two inclusions are close to each other. Fictitious frequency appearing in the exterior problem can be suppressed by using the more number of Fourier series terms. Numerical results show that the space between scatterers has the opposite effect on the near-field DMCF in comparison with the far-field scattering pattern.

© 2009 Elsevier Ltd. All rights reserved.

1. Introduction

Plates with multiple circular inclusions are commonly observed in engineering structures. These inclusions, or inhomogeneous materials, usually take place in terms of discontinuity such as thickness reduction due to corrosion, or strength degradation resulted by delamination. Dynamic loadings under the circumstance always result in stress concentration with ensuing loading capacity reduction and fatigue failure.

The deformation and corresponding stresses induced by dynamic loading are propagated throughout the structure by means of wave. At the near field of inclusion (or scatterer), flexural wave scattered in all directions recursively interacts with the incident wave. It turns out that the scattering of the stress wave results in dynamic stress concentration [1]. On the other hand, certain applications of the far-field scattering flexural response can be found in vibration analysis or structural health-monitoring system such as the non-destructive inspection.

Nishimura and Jimbo [2] are two pioneer investigators to analytically study dynamic stress concentration. They calculated the stresses in the vicinity of a spherical inclusion in the elastic solid under harmonic force. Pao [3] studied the scattering of flexural waves and dynamic stress concentrations around a circular hole, and proposed an analytical solution.

* Corresponding author.

E-mail addresses: wmllee@cc.chit.edu.tw (W.M. Lee), jtchen@mail.ntou.edu.tw (J.T. Chen).

Since then, most research has focused on the scattering of elastic wave and dynamic stress concentration and has led to a rapid development of analytical or numerical approach such as wave function expansion method, complex variable method, boundary integral equation method (BIEM), boundary element method (BEM) [1] and the method of fundamental solutions [4].

Leviatan et al. [5] presented a source-model technique for the scattering analysis of a time-harmonic flexural wave in a thin elastic plate by a small patch made of material other than that of the plate. However, the fictitious sources are located at a certain distance away from the boundary of the patch. By using the flux conservation relation and optical theorem, Norris et al. [6] considered the scattering of flexural waves by a circular inclusion with different plate properties and obtained numerical results. Squire et al. [7] applied the wave function expansion method to study the scattering properties of a single coated cylindrical anomaly located in a thin plate on which flexural waves propagate. Wang [8] presented a theoretical and experimental investigation of the scattering behavior of extensional and flexural plate waves by a cylindrical inhomogeneity. Peng [9] investigated flexural wave scattering and dynamic stress concentration in a heterogeneous plate with multiple cylindrical patches by using acoustical wave propagator technique. The predicted result of the principal stress was compared with the exact analytical solution in a thin plate without patches. Nevertheless, predicted results of dynamic stress concentration were not verified by any independent method. Recently, one monograph is devoted to discussing the multiple scattering in acoustics, electromagnetism, seismology and hydrodynamics [10].

From literature reviews stated previously, few papers except [9] have been published to date reporting the scattering of flexural wave in plate with more than one inclusion. Recently, authors proposed a semi-analytical null-field integral equation method for eigensolution of a circular plate with multiple circular holes [11]. The advantage of this approach is employing the degenerate kernel to avoid calculating principal values, which is of great difficulties in the case of plate. The introduction of degenerate kernel in companion with the Fourier series was proved to yield the exponential convergence [12] instead of the linear algebraic convergence in BEM. Furthermore, Kobayashi and Nishimura [13] pointed out that the integral equation method seems to be most effective to deal with two-dimensional steady-state flexural wave problems.

This paper extends the null-field integral approach to the exterior plate problem to solve flexural waves scattered by multiple circular inclusions. A linear algebraic system can be constructed by uniformly collocating points on the boundary and taking finite terms of Fourier series. The displacement and corresponding section force are calculated by using boundary integral equations for the domain point after determining the Fourier coefficients of unknown boundary density. For the multiply-connected plate problem, the slope (bending angle) and moment in the normal and tangential directions are determined with care in the adaptive observer system. Therefore, the operator of transformation matrix for the slope and moment is employed to deal with this problem. The results for an infinite plate with one circular inclusion are compared with the analytical solutions [6,7] to verify the validity of the proposed method. For the cases of small wave number, the quasi-static results of our propose method are confirmed by static data of finite element method (FEM) using ABAQUS [14]. Finally the effect of central distance between inclusions on the near-field DMCF and the far-field scattering pattern are also investigated.

2. Problem statement and boundary integral formulation

2.1. Problem statement

The governing equation of a uniform infinite thin plate with randomly distributed circular inclusions subject to a time-harmonic flexural wave, as shown in Fig. 1, is

$$\nabla^4 u(x) = k^4 u(x) \quad x \in \Omega \tag{1}$$

where ∇^4 is the biharmonic operator, Ω is the domain of the thin plate, $u(x)$ is the out-of-plane elastic displacement, x is the position vector of the field point in the domain, $k^4 = \omega^2 \rho_0 h / D$, k is the wave number of elastic wave, ω is the circular frequency, ρ_0 is the volume density, $D = Eh^3 / 12(1 - \mu^2)$ is the flexural rigidity, E denotes the Young's modulus, μ is the Poisson's ratio, and h is the plate thickness.

2.2. Boundary integral equation for the collocation point in the domain

The integral representation for the plate problem can be derived from the Rayleigh-Green identity [15] as follows:

$$u(x) = \int_B U(s, x) v(s) dB(s) - \int_B \Theta(s, x) m(s) dB(s) + \int_B M(s, x) \theta(s) dB(s) - \int_B V(s, x) u(s) dB(s), \quad x \in \Omega \tag{2}$$

where B is the boundary of the domain Ω , $u(s)$, $\theta(s)$, $m(s)$ and $v(s)$ are displacement, normal bending slope, bending moment and shear force of source point s along the boundary B , respectively. $U(s, x)$, $\Theta(s, x)$, $M(s, x)$ and $V(s, x)$ in Eq. (2) are kernel

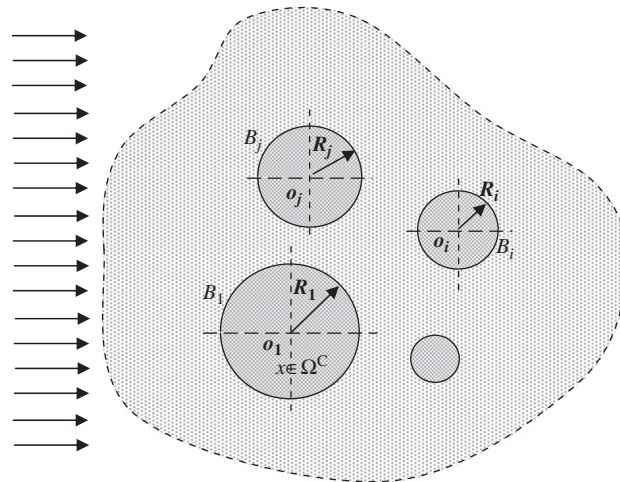


Fig. 1. Problem statement for an infinite thin plate containing multiple circular inclusions subject to an incident time-harmonic flexural wave.

functions. The kernel function $U(s, x)$ in Eq. (2),

$$U(s, x) = \frac{1}{8k^2D} \left[Y_0(kr) - iJ_0(kr) + \frac{2}{\pi} K_0(kr) \right] \quad (3)$$

is the fundamental solution [15] which satisfies

$$\nabla^4 U(s, x) - k^4 U(s, x) = \delta(s - x) \quad (4)$$

where $\delta(s - x)$ is the Dirac-delta function, $Y_0(kr)$ and $K_0(kr)$ are the zeroth-order of the second-kind Bessel and modified Bessel functions, respectively, $J_0(kr)$ is the zeroth-order of the first-kind Bessel function, $r \equiv |s - x|$ and $i^2 = -1$. The other three kernel functions, $\Theta(s, x)$, $M(s, x)$ and $V(s, x)$, in Eq. (2) can be obtained by applying the following slope, moment and effective shear operators defined by [17]

$$K_\Theta = \frac{\partial(\cdot)}{\partial n} \quad (5)$$

$$K_M = -D \left[\mu \nabla^2(\cdot) + (1 - \mu) \frac{\partial^2(\cdot)}{\partial n^2} \right] \quad (6)$$

$$K_V = -D \left[\frac{\partial}{\partial n} \nabla^2(\cdot) + (1 - \mu) \frac{\partial}{\partial t} \left(\frac{\partial}{\partial n} \left(\frac{\partial}{\partial t}(\cdot) \right) \right) \right] \quad (7)$$

to the kernel $U(s, x)$ with respect to the source point, where $\partial/\partial n$ and $\partial/\partial t$ are the normal and tangential derivatives, respectively, ∇^2 means the Laplacian operator.

2.3. Null-field integral equations

The null-field integral equations of displacement can be derived from Eq. (2) and by collocating the field point outside the domain, as follows:

$$0 = \int_B U(s, x) v(s) dB(s) - \int_B \Theta(s, x) m(s) dB(s) + \int_B M(s, x) \theta(s) dB(s) - \int_B V(s, x) u(s) dB(s), \quad x \in \Omega^C \cup B \quad (8)$$

Regarding the null-field integral equations of slope, it can be obtained by applying Eq. (5) to Eq. (8), as follow:

$$0 = \int_B U_\theta(s, x) v(s) dB(s) - \int_B \Theta_\theta(s, x) m(s) dB(s) + \int_B M_\theta(s, x) \theta(s) dB(s) - \int_B V_\theta(s, x) u(s) dB(s), \quad x \in \Omega^C \cup B \quad (9)$$

where Ω^C is the complementary domain of Ω . It is noted that once kernel functions are expressed in proper degenerate forms, which will be described in the next subsection, the collocation points can be exactly located on the real boundary, that is $x \in \Omega^C \cup B$. The other two null-field integral equations can be derived by substituting Eq. (8) into Eq. (6) and Eq. (7), respectively, and the explicit expressions can be seen in [11].

2.4. Adaptive observer system, degenerate kernels and Fourier series for boundary densities

Since the direct boundary integral equations are frame indifferent (i.e. rule of objectivity), the origin of the observer system can be adaptively located on the center of each circle under integration. In the adaptive polar coordinate, the field point x and source point s can be expressed as (ρ, ϕ) and (R, γ) , respectively. By employing the addition theorem [16], the kernel function $U(s, x)$ of Eq. (3) can be expanded in the series form as follows:

$$U : \begin{cases} U^I(s, x) = \frac{1}{8k^2D} \sum_{m=0}^{\infty} \varepsilon_m \left\{ J_m(\lambda\rho)[Y_m(kR) - iJ_m(kR)] + \frac{2}{\pi} I_m(k\rho)K_m(kR) \right\} \cos(m(\gamma - \phi)), & \rho < R \\ U^E(s, x) = \frac{1}{8k^2D} \sum_{m=0}^{\infty} \varepsilon_m \left\{ J_m(\lambda R)[Y_m(k\rho) - iJ_m(k\rho)] + \frac{2}{\pi} I_m(kR)K_m(k\rho) \right\} \cos(m(\gamma - \phi)), & \rho \geq R \end{cases} \quad (10)$$

where ε_m is the Neumann factor ($\varepsilon_m = 1, m=0; \varepsilon_m = 2, m=1, 2, \dots, \infty$) and the superscripts “I” and “E” denote the interior and exterior cases for $U(s, x)$ degenerate kernels to distinguish $\rho < R$ and $\rho > R$, respectively, as shown in Fig. 2. By comparing Eq. (10) with Eq. (3), it is noted that the variable of r , the distance between the field point and the source point, is replaced with two variables of R and ρ . By this way, the singularity does not occur when r equals to zero, i.e. the source point coincides with the field point. The advantage of using degenerate kernels in integral equations is free of calculating the principal values through a bump contour by locating the null-field point exactly on the real boundary. The degenerate kernels $\Theta(s, x)$, $M(s, x)$ and $V(s, x)$ in the null-field boundary integral equations can be obtained by applying the operators of Eqs. (5)–(7) to the degenerate kernel $U(s, x)$ with respect to the source point s .

In order to fully utilize the geometry of circular boundary, the displacement $u(s)$, slope $\theta(s)$, moment $m(s)$ and shear force $\nu(s)$ along the circular boundaries in the null-field integral equations can be expanded in terms of Fourier series, respectively, as shown below:

$$u(s) = u_{c0} + \sum_{n=1}^M (u_{cn} \cos n\gamma + u_{sn} \sin n\gamma), \quad s \in B \quad (11)$$

$$\theta(s) = \theta_{c0} + \sum_{n=1}^M (\theta_{cn} \cos n\gamma + \theta_{sn} \sin n\gamma), \quad s \in B \quad (12)$$

$$m(s) = m_{c0} + \sum_{n=1}^M (m_{cn} \cos n\gamma + m_{sn} \sin n\gamma), \quad s \in B \quad (13)$$

$$\nu(s) = \nu_{c0} + \sum_{n=1}^M (\nu_{cn} \cos n\gamma + \nu_{sn} \sin n\gamma), \quad s \in B \quad (14)$$

where $u_{c0}, u_{cn}, u_{sn}, \theta_{c0}, \theta_{cn}, \theta_{sn}, m_{c0}, m_{cn}, m_{sn}, \nu_{c0}, \nu_{cn}$ and ν_{sn} are the Fourier coefficients and M is the truncated number of Fourier series terms.

Fig. 3 shows the circular boundary integration in the adaptive observer system. The dummy variable in the circular contour integration is the angle (γ) instead of radial coordinate (R). By using the orthogonal property between degenerate kernels and Fourier series, all the improper boundary integrals in Eqs. (8)–(9) can be transformed to series sum and then be

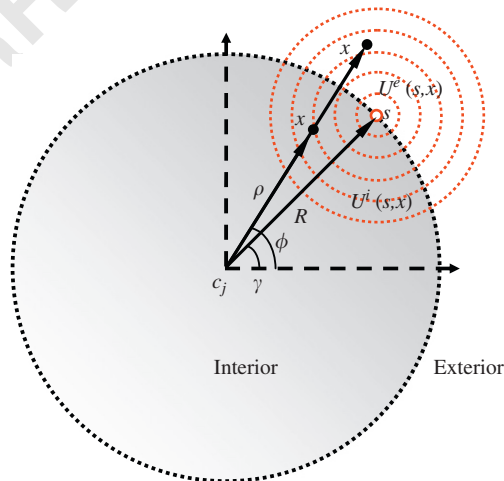
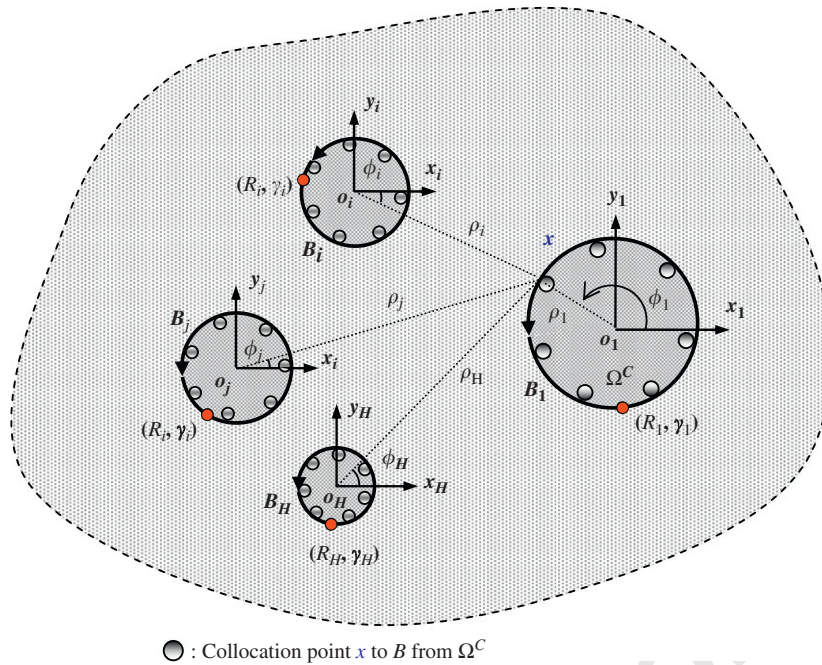


Fig. 2. Degenerate kernel for $U(s, x)$.



● : Collocation point x to B from Ω^C

Fig. 3. Collocation point and boundary contour integration in the boundary integral equation for the plate by using the adaptive observer system.

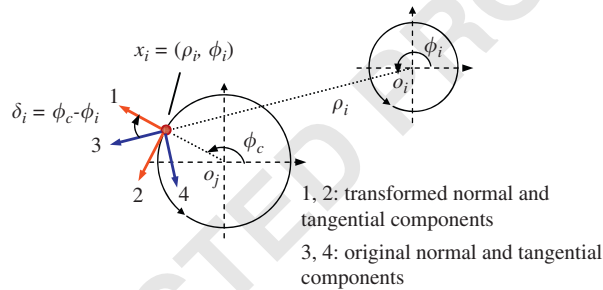


Fig. 4. Transformation of tensor components.

determined analytically free of principal value sense. By comparing Eq. (10) with Eq. (3), it is noted that the variable r , $|x-s|$, is replaced with the variables, R and ρ . Consequently, the singularity will not occur when the collocation points are exactly located on the real boundary and the source point coincides with the field point, i.e. $r=0$.

3. Transformation of tensor components

For the case of multiple inclusions, it is inevitable that the source and field points locate on different circular boundaries. The calculated boundary data such as the slope, moment and effective shear force should be transformed to the direction where the specified boundary conditions are given. As shown in Fig. 4, ϕ_i is the angle of the collocation point x_i with respect to o_i , which is center of the circle under integration, ϕ_c is that with respect to o_j , which is center of the circle on which collocation point is located. According to the transformation law for the components of tensor, we have

$$\begin{bmatrix} (\cdot)_n \\ (\cdot)_t \end{bmatrix} = \begin{bmatrix} \cos(\delta) & \sin(\delta) \\ -\sin(\delta) & \cos(\delta) \end{bmatrix} \begin{bmatrix} (\cdot)_\rho \\ (\cdot)_\phi \end{bmatrix} \tag{15}$$

$$\begin{bmatrix} (\cdot)_{nn} \\ (\cdot)_{tt} \\ (\cdot)_{nt} \end{bmatrix} = \begin{bmatrix} \cos^2(\delta) & \sin^2(\delta) & 2 \sin(\delta) \cos(\delta) \\ \sin^2(\delta) & \cos^2(\delta) & -2 \sin(\delta) \cos(\delta) \\ -\sin(\delta) \cos(\delta) & \sin(\delta) \cos(\delta) & \cos^2(\delta) - \sin^2(\delta) \end{bmatrix} \begin{bmatrix} (\cdot)_{\rho\rho} \\ (\cdot)_{\phi\phi} \\ (\cdot)_{\rho\phi} \end{bmatrix} \tag{16}$$

Based on Eqs. (15) and (16), the general rotated slope and tangential bending moment kernels can be obtained by following operators:

$$K_{\theta}^R = \cos(\delta) \frac{\partial(\cdot)}{\partial n} + \sin(\delta) \frac{\partial(\cdot)}{\partial t} \tag{17}$$

$$K_T^R = -D \left\{ [\mu + (1 - \mu) \cos^2(\delta)] \nabla^2(\cdot) + \cos(2\delta)(\mu - 1) \frac{\partial^2(\cdot)}{\partial n^2} - \sin(2\delta)(1 - \mu) \frac{\partial}{\partial n} \left(\frac{\partial(\cdot)}{\partial t} \right) \right\} \tag{18}$$

where $\delta = \phi_c - \phi_i$. When ϕ_c equals to ϕ_i or the angle difference δ equals to zero, Eq. (17) is simplified to Eq. (5). The expressions of rotated degenerate kernels, $U_{\theta}(s, x)$, $\Theta_{\theta}(s, x)$, $M_{\theta}(s, x)$, $U_t(s, x)$, $\Theta_t(s, x)$, $M_t(s, x)$ and $V_t(s, x)$, can be obtained by applying the operators of Eqs. (17) and (18) to the degenerate kernel $U(s, x)$, $\Theta(s, x)$, $M(s, x)$ and $V(s, x)$ with respect to the field point x .

4. Linear algebraic systems

Consider an infinite plate containing H non-overlapping circular inclusions shown in Fig. 3, where x is the collocation point, $o_j (j=1,2,\dots,H)$ is the position vector of each center of circular inclusions, R_j and B_j denote the radius and the boundary of the j th circular inclusion, respectively. Since the four null field integral equations [11] in the plate formulation are provided, there are 6 (C_2^4) options of choosing any two equations to solve the problems. For the purpose of computational efficiency, Eqs. (8) and (9) are used to analyze the plate problem. By uniformly collocating $N (=2M+1)$ points on each circular boundary in Eqs. (8) and (9), we have

$$0 = \sum_{j=1}^H \int_{B_j} \int_{B_j} \{U(s, x)v(s) - \Theta(s, x)m(s) + M(s, x)\theta(s) - V(s, x)u(s)\} dB_j(s), \quad x \in \Omega^C \cup B \tag{19}$$

$$0 = \sum_{j=1}^H \int_{B_j} \{U_{\theta}(s, x)v(s) - \Theta_{\theta}(s, x)m(s) + M_{\theta}(s, x)\theta(s) - V_{\theta}(s, x)u(s)\} dB_j(s), \quad x \in \Omega^C \cup B \tag{20}$$

In the B_j integration, the origin of the observer system is adaptively located at the center o_j from which the degenerate kernels and Fourier series are described. The selection of interior or exterior degenerate kernel depends on $\rho < R$ or $\rho > R$, respectively, according to the observer system. By using orthogonal property, a linear algebraic system can be written as follows:

$$\begin{bmatrix} U^{11} & -\Theta^{11} & U^{12} & -\Theta^{12} & \dots & U^{1H} & -\Theta^{1H} \\ U_{\theta}^{11} & -\Theta_{\theta}^{11} & U_{\theta}^{12} & -\Theta_{\theta}^{12} & \dots & U_{\theta}^{1H} & -\Theta_{\theta}^{1H} \\ U^{21} & -\Theta^{21} & U^{22} & -\Theta^{22} & \dots & U^{2H} & -\Theta^{2H} \\ U_{\theta}^{21} & -\Theta_{\theta}^{21} & U_{\theta}^{22} & -\Theta_{\theta}^{22} & \dots & U_{\theta}^{2H} & -\Theta_{\theta}^{2H} \\ \vdots & \vdots & \vdots & \vdots & \ddots & \vdots & \vdots \\ U^{H1} & -\Theta^{H1} & U_{\theta}^{H2} & -\Theta_{\theta}^{H2} & \dots & U^{HH} & -\Theta^{HH} \\ U_{\theta}^{H1} & -\Theta_{\theta}^{H1} & U_{\theta}^{H2} & -\Theta_{\theta}^{H2} & \dots & U_{\theta}^{HH} & -\Theta_{\theta}^{HH} \end{bmatrix} \begin{Bmatrix} v^1 \\ m^1 \\ v^2 \\ m^2 \\ \vdots \\ v^H \\ m^H \end{Bmatrix} = \begin{bmatrix} -M^{11} & V^{11} & -M^{12} & V^{12} & \dots & -M^{1H} & V^{1H} \\ -M_{\theta}^{11} & V_{\theta}^{11} & -M_{\theta}^{12} & V_{\theta}^{12} & \dots & -M_{\theta}^{1H} & V_{\theta}^{1H} \\ -M^{21} & V^{21} & -M^{22} & V^{22} & \dots & -M^{2H} & V^{2H} \\ -M_{\theta}^{21} & V_{\theta}^{21} & -M_{\theta}^{22} & V_{\theta}^{22} & \dots & -M_{\theta}^{2H} & V_{\theta}^{2H} \\ \vdots & \vdots & \vdots & \vdots & \ddots & \vdots & \vdots \\ -M^{H1} & V^{H1} & -M_{\theta}^{H2} & V_{\theta}^{H2} & \dots & -M^{HH} & V^{HH} \\ -M_{\theta}^{H1} & V_{\theta}^{H1} & -M_{\theta}^{H2} & V_{\theta}^{H2} & \dots & -M_{\theta}^{HH} & V_{\theta}^{HH} \end{bmatrix} \begin{Bmatrix} \theta^1 \\ u^1 \\ \theta^2 \\ u^2 \\ \vdots \\ \theta^H \\ u^H \end{Bmatrix} \tag{21}$$

For brevity, a unified form $[U^{ij}] (i = 1, 2, 3, \dots, H$ and $j = 1, 2, 3, \dots, H)$ denote the response of $U(s, x)$ kernel at the i th circle point due to the source at the j th circle. Otherwise, the same definition is for $[\Theta^{ij}]$, $[M^{ij}]$, $[V^{ij}]$, $[U_{\theta}^{ij}]$, $[\Theta_{\theta}^{ij}]$, $[M_{\theta}^{ij}]$ and $[V_{\theta}^{ij}]$ kernels. The explicit expressions for sub-vectors $[u^i]$, $[\theta^i]$, $[m^i]$ and $[v^i]$ can be described as follows:

$$u^i = \begin{Bmatrix} u_{c0}^i \\ u_{c1}^i \\ u_{s1}^i \\ \vdots \\ u_{cM}^i \\ u_{sM}^i \end{Bmatrix}, \quad \theta^i = \begin{Bmatrix} \theta_{c0}^i \\ \theta_{c1}^i \\ \theta_{s1}^i \\ \vdots \\ \theta_{cM}^i \\ \theta_{sM}^i \end{Bmatrix}, \quad m^i = \begin{Bmatrix} m_{c0}^i \\ m_{c1}^i \\ m_{s1}^i \\ \vdots \\ m_{cM}^i \\ m_{sM}^i \end{Bmatrix}, \quad v^i = \begin{Bmatrix} v_{c0}^i \\ v_{c1}^i \\ v_{s1}^i \\ \vdots \\ v_{cM}^i \\ v_{sM}^i \end{Bmatrix} \tag{22}$$

The explicit expressions for the sub-matrices of $[U^{ij}]$, $[\Theta^{ij}]$, $[M^{ij}]$, $[V^{ij}]$, $[U_{\theta}^{ij}]$, $[\Theta_{\theta}^{ij}]$, $[M_{\theta}^{ij}]$ and $[V_{\theta}^{ij}]$ can be written as shown below:

$$K^{ij} = \begin{bmatrix} K_{0C}^{ij}(\rho_1, \phi_1) & K_{1C}^{ij}(\rho_1, \phi_1) & K_{1S}^{ij}(\rho_1, \phi_1) & \cdots & K_{MS}^{ij}(\rho_1, \phi_1) \\ K_{0C}^{ij}(\rho_2, \phi_2) & K_{1C}^{ij}(\rho_2, \phi_2) & K_{1S}^{ij}(\rho_2, \phi_2) & \cdots & K_{MS}^{ij}(\rho_2, \phi_2) \\ \vdots & \vdots & \vdots & \ddots & \vdots \\ K_{0C}^{ij}(\rho_N, \phi_N) & K_{1C}^{ij}(\rho_N, \phi_N) & K_{1S}^{ij}(\rho_N, \phi_N) & \cdots & K_{MS}^{ij}(\rho_N, \phi_N) \end{bmatrix}_{N \times N} \quad (23)$$

where K can be either one of $U(s, x)$, $\Theta(s, x)$, $M(s, x)$, $V(s, x)$, $U_{\theta}(s, x)$, $\Theta_{\theta}(s, x)$, $M_{\theta}(s, x)$ and $V_{\theta}(s, x)$. The notations ϕ_k and ρ_k ($k = 1, 2, 3, \dots, N$) shown in Fig. 3 are the angle and radius of the k -th collocation point on the i -th circular boundary with respect to the center of the j -th circular boundary (the origin of the observer system) and the element of the sub-matrices can be determined by

$$K_{nC}^{ij}(\rho_k, \phi_k) = \int_0^{2\pi} K(R_j, \gamma_j; \rho_k, \phi_k) \cos(n\gamma_j)(R_j d\gamma_j), \quad n = 0, 1, 2, \dots, M \quad (24)$$

$$K_{nS}^{ij}(\rho_k, \phi_k) = \int_0^{2\pi} K(R_j, \gamma_j; \rho_k, \phi_k) \sin(n\gamma_j)(R_j d\gamma_j), \quad n = 1, 2, \dots, M \quad (25)$$

5. Techniques for solving scattering problems of inclusions

For an infinite thin plate with H circular inclusions subject to an incident flexural wave, the systems for surrounding plate, or matrix, and inclusions can be represented, respectively, as follows:

$$\begin{bmatrix} U^{M_{11}} & -\Theta^{M_{11}} & \cdots & U^{M_{1H}} & -\Theta^{M_{1H}} \\ U_{\theta}^{M_{11}} & -\Theta_{\theta}^{M_{11}} & \cdots & U_{\theta}^{M_{1H}} & -\Theta_{\theta}^{M_{1H}} \\ \vdots & \vdots & \ddots & \vdots & \vdots \\ U^{M_{H1}} & -\Theta^{M_{H1}} & \cdots & U^{M_{HH}} & -\Theta^{M_{HH}} \\ U_{\theta}^{M_{H1}} & -\Theta_{\theta}^{M_{H1}} & \cdots & U_{\theta}^{M_{HH}} & -\Theta_{\theta}^{M_{HH}} \end{bmatrix} \begin{Bmatrix} v_1^{sc} \\ m_1^{sc} \\ \vdots \\ v_H^{sc} \\ m_H^{sc} \end{Bmatrix} + \begin{bmatrix} M^{M_{11}} & -V^{M_{11}} & \cdots & M^{M_{1H}} & -V^{M_{1H}} \\ M_{\theta}^{M_{11}} & -V_{\theta}^{M_{11}} & \cdots & M_{\theta}^{M_{1H}} & -V_{\theta}^{M_{1H}} \\ \vdots & \vdots & \ddots & \vdots & \vdots \\ M^{M_{H1}} & -V^{M_{H1}} & \cdots & M^{M_{HH}} & -V^{M_{HH}} \\ M_{\theta}^{M_{H1}} & -V_{\theta}^{M_{H1}} & \cdots & M_{\theta}^{M_{HH}} & -V_{\theta}^{M_{HH}} \end{bmatrix} \begin{Bmatrix} \theta_1^{sc} \\ u_1^{sc} \\ \vdots \\ \theta_H^{sc} \\ u_H^{sc} \end{Bmatrix} = 0 \quad (26)$$

$$\begin{bmatrix} U^I & -\Theta^I \\ U_{\theta}^I & -\Theta_{\theta}^I \end{bmatrix} \begin{Bmatrix} v_j \\ m_j \end{Bmatrix} + \begin{bmatrix} M^I & -V^I \\ M_{\theta}^I & -V_{\theta}^I \end{bmatrix} \begin{Bmatrix} \theta_j \\ u_j \end{Bmatrix} = 0, \quad j = 1, \dots, H \quad (27)$$

where the subscript j denotes the j th circular inclusion, the superscript M and I denote the matrix and inclusion, respectively, the superscript sc denotes the scattered field from the boundary between plate and inclusion. The displacement u_j , slope θ_j , moment m_j and shear force v_j are unknown variables along each circular boundary B_j ($j=1, \dots, H$). For the scattering plate problem with an uncoated circular inclusion, it can be further decomposed into three parts (a) an interior circular inclusion problem, (b) an exterior scattering plate problem and (c) the incident wave field, as shown in Fig. 5. For satisfying the continuity conditions of displacement, slope, normal bending moment and effective shear on the each circular boundary, the scattering boundary conditions in part (b) are

$$u_j^{sc} = u_j - u_j^i, \quad j = 1, \dots, H \quad (28)$$

$$\theta_j^{sc} = \theta_j - \theta_j^i, \quad j = 1, \dots, H \quad (29)$$

$$m_j^{sc} = m_j - m_j^i, \quad j = 1, \dots, H \quad (30)$$

$$v_j^{sc} = v_j - v_j^i, \quad j = 1, \dots, H \quad (31)$$

where the subscript i denotes the incident wave. By substituting Eqs. (28)–(31) into Eq. (26) and then combining with Eq. (27), the system for an infinite plate containing two uncoated circular inclusions, for instance, can be

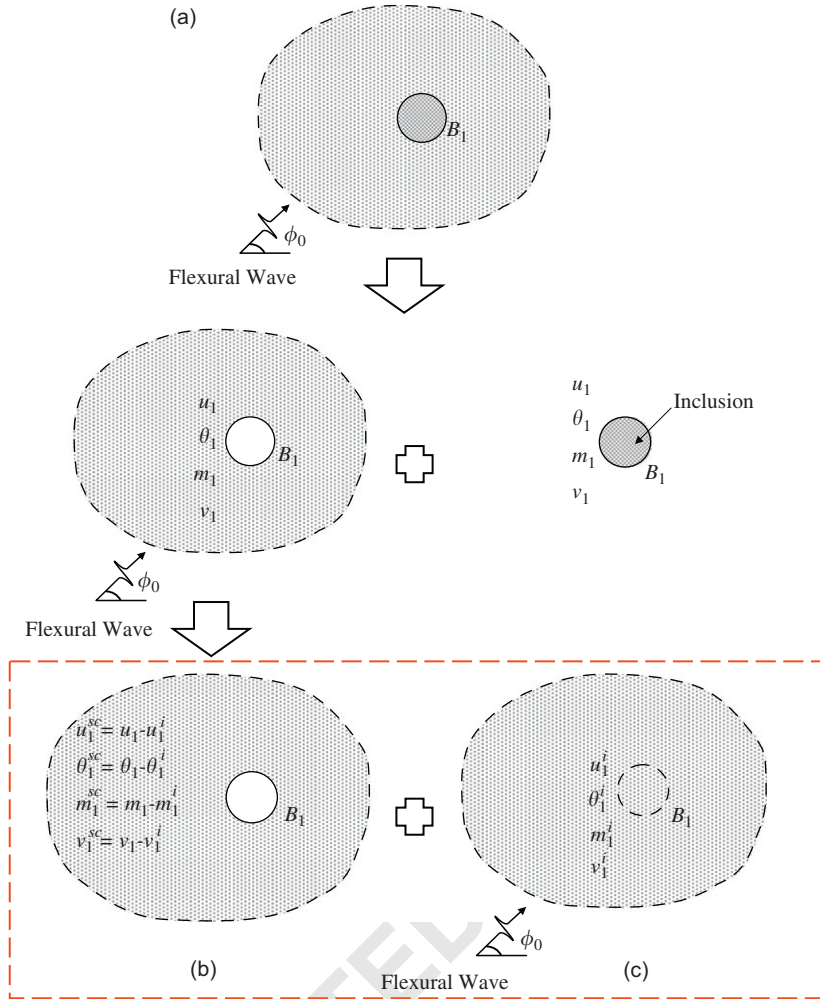


Fig. 5. Decomposition of scattering plate problem with an uncoated inclusion into (a) an interior circular inclusion problem, (b) an exterior scattering plate problem and (c) the incident wave field.

represented as

$$\begin{bmatrix}
 U^{M11} & -\Theta^{M11} & M^{M11} & -V^{M11} & U^{M12} & -\Theta^{M12} & M^{M12} & -V^{M12} \\
 U_{\theta}^{M11} & -\Theta_{\theta}^{M11} & M_{\theta}^{M11} & -V_{\theta}^{M11} & U_{\theta}^{M12} & -\Theta_{\theta}^{M12} & M_{\theta}^{M12} & -V_{\theta}^{M12} \\
 U^{I1} & -\Theta^{I1} & M^{I1} & -V^{I1} & 0 & 0 & 0 & 0 \\
 U_{\theta}^{I1} & -\Theta_{\theta}^{I1} & M_{\theta}^{I1} & -V_{\theta}^{I1} & 0 & 0 & 0 & 0 \\
 U^{M21} & -\Theta^{M21} & M^{M21} & -V^{M21} & U^{M22} & -\Theta^{M22} & M^{M22} & -V^{M22} \\
 U_{\theta}^{M21} & -\Theta_{\theta}^{M21} & M_{\theta}^{M21} & -V_{\theta}^{M21} & U_{\theta}^{M22} & -\Theta_{\theta}^{M22} & M_{\theta}^{M22} & -V_{\theta}^{M22} \\
 0 & 0 & 0 & 0 & U^{I2} & -\Theta^{I2} & M^{I2} & -V^{I2} \\
 0 & 0 & 0 & 0 & U_{\theta}^{I2} & -\Theta_{\theta}^{I2} & M_{\theta}^{I2} & -V_{\theta}^{I2}
 \end{bmatrix}
 \begin{Bmatrix}
 v_1 \\
 m_1 \\
 \theta_1 \\
 u_1 \\
 v_2 \\
 m_2 \\
 \theta_2 \\
 u_2
 \end{Bmatrix}
 =
 \begin{Bmatrix}
 f_1^v \\
 f_1^m \\
 0 \\
 0 \\
 f_2^v \\
 f_2^m \\
 0 \\
 0
 \end{Bmatrix}
 \quad (32)$$

where

$$f_1^v = U^{M11} v_1^i - \Theta^{M11} m_1^i + M^{M11} \theta_1^i - V^{M11} u_1^i + U^{M12} v_2^i - \Theta^{M12} m_2^i + M^{M12} \theta_2^i - V^{M12} u_2^i \quad (33)$$

$$f_1^m = U_{\theta}^{M11} v_1^i - \Theta_{\theta}^{M11} m_1^i + M_{\theta}^{M11} \theta_1^i - V_{\theta}^{M11} u_1^i + U_{\theta}^{M12} v_2^i - \Theta_{\theta}^{M12} m_2^i + M_{\theta}^{M12} \theta_2^i - V_{\theta}^{M12} u_2^i \quad (34)$$

$$f_2^v = U^{M21} v_1^i - \Theta^{M21} m_1^i + M^{M21} \theta_1^i - V^{M21} u_1^i + U^{M22} v_2^i - \Theta^{M22} m_2^i + M^{M22} \theta_2^i - V^{M22} u_2^i \quad (35)$$

$$f_2^m = U_{\theta}^{M21} v_1^i - \Theta_{\theta}^{M21} m_1^i + M_{\theta}^{M21} \theta_1^i - V_{\theta}^{M21} u_1^i + U_{\theta}^{M22} v_2^i - \Theta_{\theta}^{M22} m_2^i + M_{\theta}^{M22} \theta_2^i - V_{\theta}^{M22} u_2^i \quad (36)$$

For the coated inclusion shown in Fig. 6, i.e. the inclusion being coated some material other than the surrounding plate, the system for an infinite plate containing two coated circular inclusions, for instance, can be represented by

$$\begin{bmatrix}
 U^{M_{11}} & -\Theta^{M_{11}} & M^{M_{11}} & -V^{M_{11}} & 0 & 0 & 0 & 0 & 0 & 0 & U^{M_{13}} & -\Theta^{M_{13}} & M^{M_{13}} & -V^{M_{13}} & 0 & 0 & 0 & 0 \\
 U_{\theta}^{M_{11}} & -\Theta_{\theta}^{M_{11}} & M_{\theta}^{M_{11}} & -V_{\theta}^{M_{11}} & 0 & 0 & 0 & 0 & 0 & 0 & U_{\theta}^{M_{13}} & -\Theta_{\theta}^{M_{13}} & M_{\theta}^{M_{13}} & -V_{\theta}^{M_{13}} & 0 & 0 & 0 & 0 \\
 U^{I_{11}} & -\Theta^{I_{11}} & M^{I_{11}} & -V^{I_{11}} & U^{I_{12}} & -\Theta^{I_{12}} & M^{I_{12}} & -V^{I_{12}} & 0 & 0 & 0 & 0 & 0 & 0 & 0 & 0 & 0 & 0 \\
 U_{\theta}^{I_{11}} & -\Theta_{\theta}^{I_{11}} & M_{\theta}^{I_{11}} & -V_{\theta}^{I_{11}} & U_{\theta}^{I_{12}} & -\Theta_{\theta}^{I_{12}} & M_{\theta}^{I_{12}} & -V_{\theta}^{I_{12}} & 0 & 0 & 0 & 0 & 0 & 0 & 0 & 0 & 0 & 0 \\
 U^{I_{21}} & -\Theta^{I_{21}} & M^{I_{21}} & -V^{I_{21}} & U^{I_{22}} & -\Theta^{I_{22}} & M^{I_{22}} & -V^{I_{22}} & 0 & 0 & 0 & 0 & 0 & 0 & 0 & 0 & 0 & 0 \\
 U_{\theta}^{I_{21}} & -\Theta_{\theta}^{I_{21}} & M_{\theta}^{I_{21}} & -V_{\theta}^{I_{21}} & U_{\theta}^{I_{22}} & -\Theta_{\theta}^{I_{22}} & M_{\theta}^{I_{22}} & -V_{\theta}^{I_{22}} & 0 & 0 & 0 & 0 & 0 & 0 & 0 & 0 & 0 & 0 \\
 0 & 0 & 0 & 0 & U^{I_2} & -\Theta^{I_2} & M^{I_2} & -V^{I_2} & 0 & 0 & 0 & 0 & 0 & 0 & 0 & 0 & 0 & 0 \\
 0 & 0 & 0 & 0 & U_{\theta}^{I_2} & -\Theta_{\theta}^{I_2} & M_{\theta}^{I_2} & -V_{\theta}^{I_2} & 0 & 0 & 0 & 0 & 0 & 0 & 0 & 0 & 0 & 0 \\
 U^{M_{31}} & -\Theta^{M_{31}} & M^{M_{31}} & -V^{M_{31}} & 0 & 0 & 0 & 0 & 0 & 0 & U^{M_{33}} & -\Theta^{M_{33}} & M^{M_{33}} & -V^{M_{33}} & 0 & 0 & 0 & 0 \\
 U_{\theta}^{M_{31}} & -\Theta_{\theta}^{M_{31}} & M_{\theta}^{M_{31}} & -V_{\theta}^{M_{31}} & 0 & 0 & 0 & 0 & 0 & 0 & U_{\theta}^{M_{33}} & -\Theta_{\theta}^{M_{33}} & M_{\theta}^{M_{33}} & -V_{\theta}^{M_{33}} & 0 & 0 & 0 & 0 \\
 0 & 0 & 0 & 0 & 0 & 0 & 0 & 0 & 0 & 0 & U^{I_{33}} & -\Theta^{I_{33}} & M^{I_{33}} & -V^{I_{33}} & U^{I_{34}} & -\Theta^{I_{34}} & M^{I_{34}} & -V^{I_{34}} \\
 0 & 0 & 0 & 0 & 0 & 0 & 0 & 0 & 0 & 0 & U_{\theta}^{I_{33}} & -\Theta_{\theta}^{I_{33}} & M_{\theta}^{I_{33}} & -V_{\theta}^{I_{33}} & U_{\theta}^{I_{34}} & -\Theta_{\theta}^{I_{34}} & M_{\theta}^{I_{34}} & -V_{\theta}^{I_{34}} \\
 0 & 0 & 0 & 0 & 0 & 0 & 0 & 0 & 0 & 0 & U^{I_{43}} & -\Theta^{I_{43}} & M^{I_{43}} & -V^{I_{43}} & U^{I_{44}} & -\Theta^{I_{44}} & M^{I_{44}} & -V^{I_{44}} \\
 0 & 0 & 0 & 0 & 0 & 0 & 0 & 0 & 0 & 0 & U_{\theta}^{I_{43}} & -\Theta_{\theta}^{I_{43}} & M_{\theta}^{I_{43}} & -V_{\theta}^{I_{43}} & U_{\theta}^{I_{44}} & -\Theta_{\theta}^{I_{44}} & M_{\theta}^{I_{44}} & -V_{\theta}^{I_{44}} \\
 0 & 0 & 0 & 0 & 0 & 0 & 0 & 0 & 0 & 0 & 0 & 0 & 0 & 0 & U^{I_4} & -\Theta^{I_4} & M^{I_4} & -V^{I_4} \\
 0 & 0 & 0 & 0 & 0 & 0 & 0 & 0 & 0 & 0 & 0 & 0 & 0 & 0 & U_{\theta}^{I_4} & -\Theta_{\theta}^{I_4} & M_{\theta}^{I_4} & -V_{\theta}^{I_4}
 \end{bmatrix}
 \begin{Bmatrix}
 v_1 \\
 m_1 \\
 \theta_1 \\
 u_1 \\
 v_2 \\
 m_2 \\
 \theta_2 \\
 u_2 \\
 v_3 \\
 m_3 \\
 \theta_3 \\
 u_3 \\
 v_4 \\
 m_4 \\
 \theta_4 \\
 u_4
 \end{Bmatrix}
 =
 \begin{Bmatrix}
 f_1^v \\
 f_1^m \\
 0 \\
 0 \\
 0 \\
 0 \\
 0 \\
 0 \\
 f_3^v \\
 f_3^m \\
 0 \\
 0 \\
 0 \\
 0 \\
 0 \\
 0 \\
 0 \\
 0
 \end{Bmatrix}
 \quad (37)$$

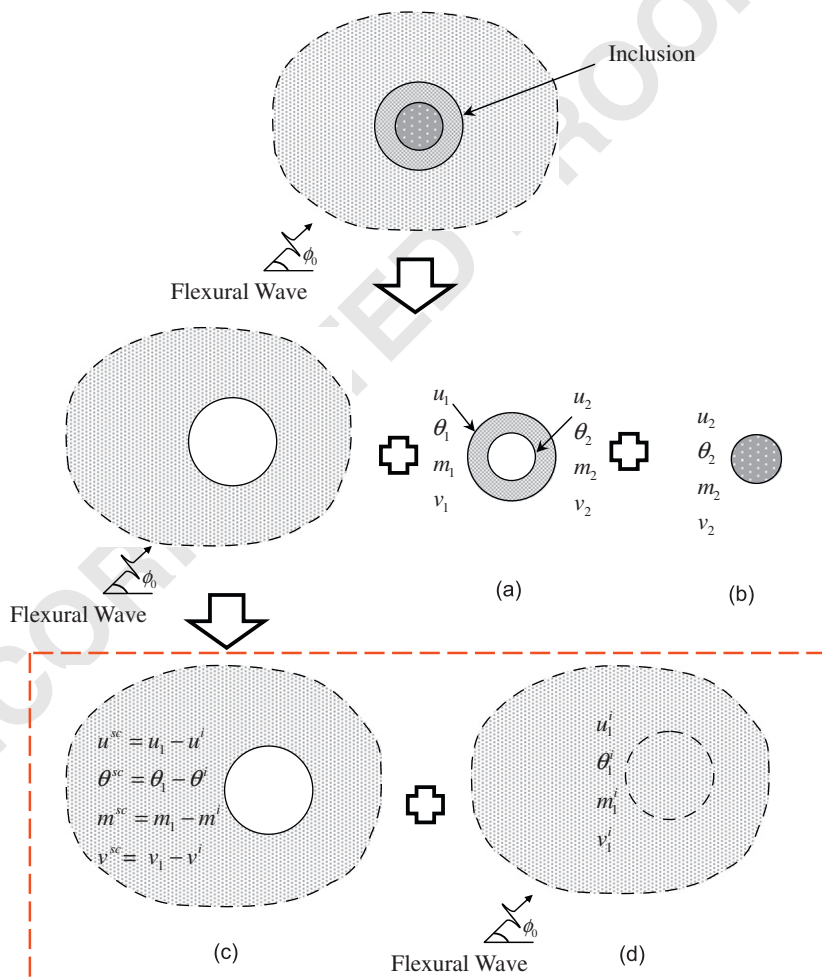


Fig. 6. Decomposition of scattering plate problem with a coated inclusion into (a) an interior annular inclusion problem, (b) an interior circular inclusion problem, (c) an exterior scattering plate problem and (d) incident wave field.

where

$$f_1^v = U^{M_{11}} v_1^i - \Theta^{M_{11}} m_1^i + M^{M_{11}} \theta_1^i - V^{M_{11}} u_1^i + U^{M_{13}} v_3^i - \Theta^{M_{13}} m_3^i + M^{M_{13}} \theta_3^i - V^{M_{13}} u_3^i \quad (38)$$

$$f_1^m = U_\theta^{M_{11}} v_1^i - \Theta_\theta^{M_{11}} m_1^i + M_\theta^{M_{11}} \theta_1^i - V_\theta^{M_{11}} u_1^i + U_\theta^{M_{13}} v_3^i - \Theta_\theta^{M_{13}} m_3^i + M_\theta^{M_{13}} \theta_3^i - V_\theta^{M_{13}} u_3^i \quad (39)$$

$$f_3^v = U^{M_{31}} v_1^i - \Theta^{M_{31}} m_1^i + M^{M_{31}} \theta_1^i - V^{M_{31}} u_1^i + U^{M_{33}} v_3^i - \Theta^{M_{33}} m_3^i + M^{M_{33}} \theta_3^i - V^{M_{33}} u_3^i \quad (40)$$

$$f_3^m = U_\theta^{M_{31}} v_1^i - \Theta_\theta^{M_{31}} m_1^i + M_\theta^{M_{31}} \theta_1^i - V_\theta^{M_{31}} u_1^i + U_\theta^{M_{33}} v_3^i - \Theta_\theta^{M_{33}} m_3^i + M_\theta^{M_{33}} \theta_3^i - V_\theta^{M_{33}} u_3^i \quad (41)$$

After calculating the displacement, slope, moment and effective shear force along the boundary, the scattered field can be solved by employing the boundary integral equation for the domain point. The total field is determined by superimposing the scattered field and the incident field as follow:

$$u = u^{sc} + u^i \quad (42)$$

The tangential bending moment $M_t(x)$ can be determined by applying the operator of Eq. (19) to the total field with respective to the field point.

5.1. Dynamic moment concentration factor

An incident flexural wave is represented by

$$u^i = u_0^i e^{ik(x \cos(\phi_0) + y \sin(\phi_0))} \quad (43)$$

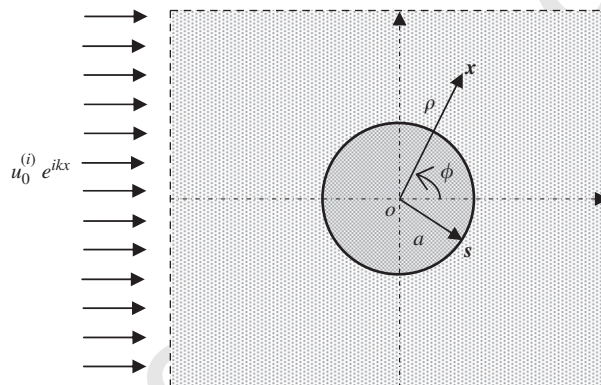


Fig. 7. An infinite plate containing an uncoated inclusion subject to an incident flexural wave.

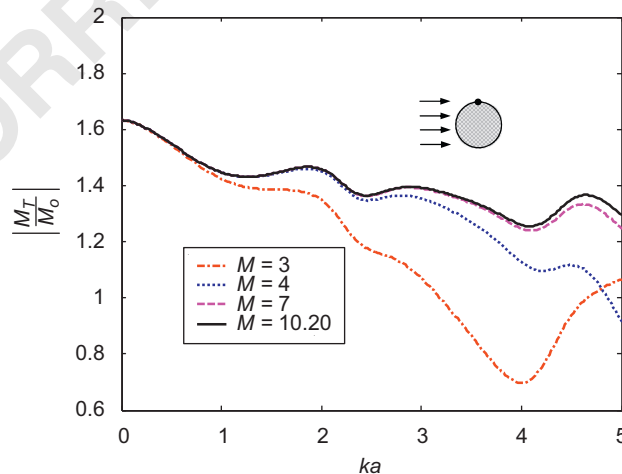


Fig. 8. Dynamic moment concentration factor on the circular boundary ($\gamma=\pi/2$) versus the dimensionless wave number by using different number of terms of Fourier series.

where u_0^i is the amplitude of incident wave, k is the wave number and ϕ_0 is the incident angle. Under the polar coordinate, the bending moment and effective shear force induced by the incident wave can be determined by substituting Eq. (43) into Eqs. (6) and (7). By setting the amplitude of incident wave $u_0^i = 1$, the amplitude of moment produced by the incident

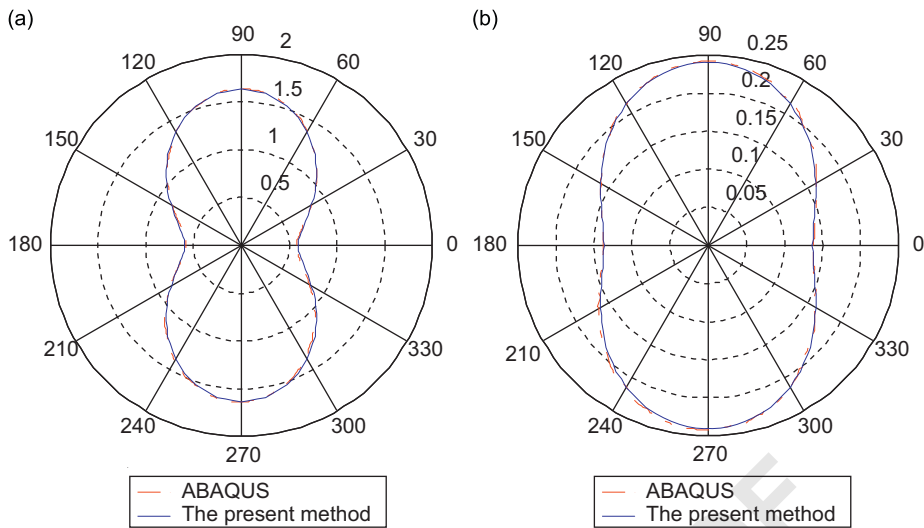


Fig. 9. Distribution of dynamic moment concentration factors on the circular boundary of the matrix and inclusion by using the present method ($M=4$, $ka=0.005$) and FEM (ABAQUS, under static loading).

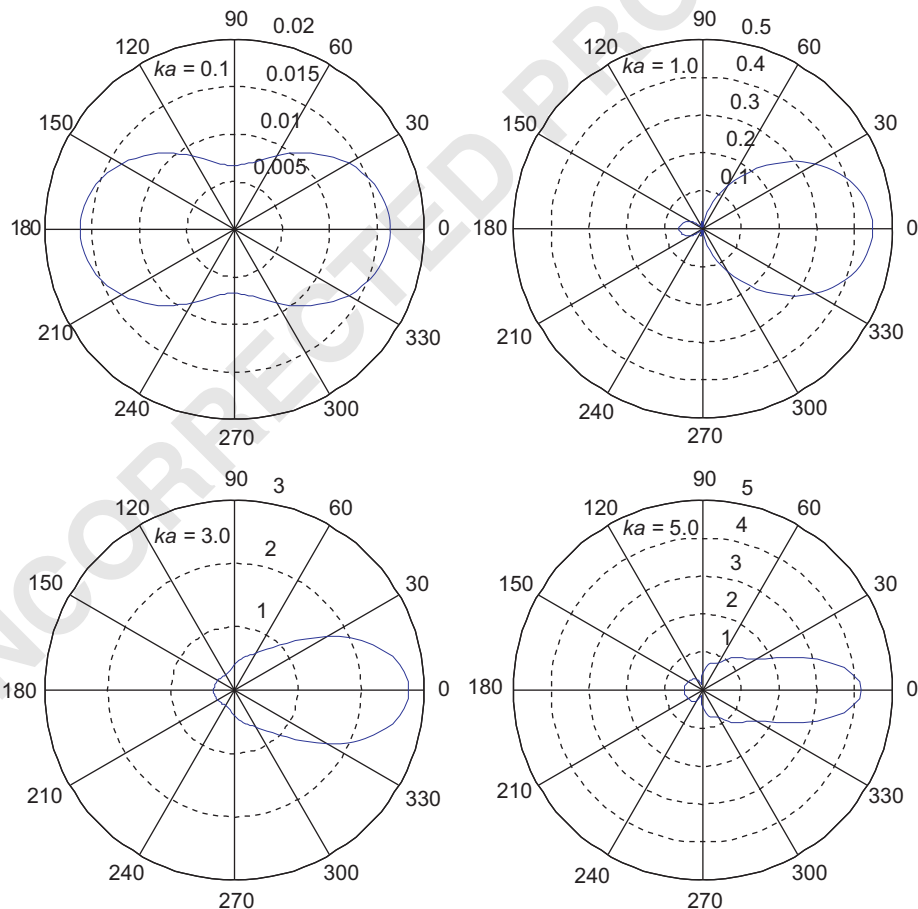


Fig. 10. Far-field scattering pattern for a flexible inclusion with $h_1=h/2$ at different dimensionless wave numbers $ka=0.1, 1.0, 3.0$ and 5.0 .

1 wave is

$$M_0 = Dk^2 \quad (44)$$

3 The dynamic moment concentration factor (DMCF) at any field point x can be determined as

$$DMCF(x) = M_t(x)/M_0 \quad (45)$$

7 5.2. Scattered far-field amplitude

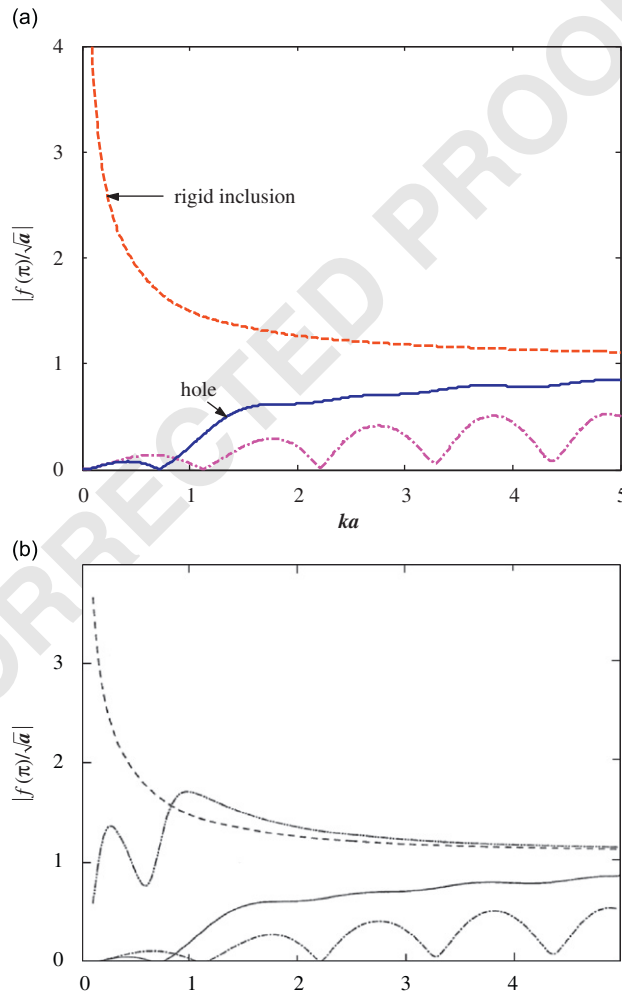
9 For the most part of scattering applications, it is interesting to measure the scattered field far away from the scatter. On the other hand, the asymptotic behavior or uniqueness of fundamental solutions is an important issue for the numerical computation. Therefore, we examine the behavior of the scattered response in the far field. The scattered far-field amplitude $f(\theta)$ [5] in our approach is defined as

$$f(\theta) = \lim_{\rho \rightarrow \infty} \sqrt{2\rho} \cdot u^{sc}(\rho) \quad (46)$$

15 where $u^{sc}(\rho)$ is the out-of-plane elastic displacement of scattered field, ρ is the radius of the field point.

17 6. Numerical results and discussions

19 The following numerical simulation utilizes the proposed method for finding dynamic moment concentration factor (DMCF) around circular inclusions as well as the scattered far-field amplitude. For the cases of small wave number, the



23 **Fig. 11.** Far-field backscattering amplitude versus the dimensionless wave number by using (a) the present method and (b) the method of Norris et al. [6], where the surrounding plate is steel of thickness 0.025 m, solid line for the hole, dashed line for the rigid inclusion and dash-dot line for the inclusion with thickness 0.0125 m.

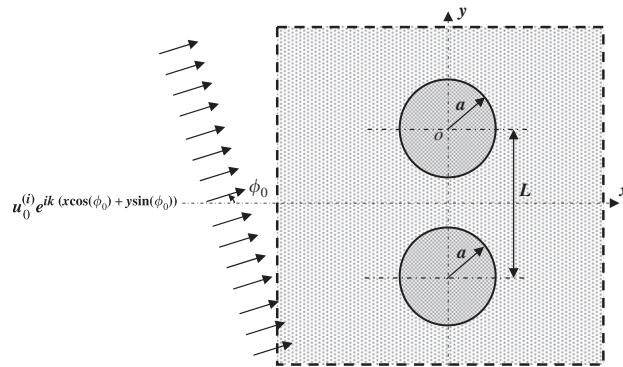


Fig. 12. An infinite plate with two uncoated inclusions subject to an incident flexural wave with an incident angle ϕ_0 .

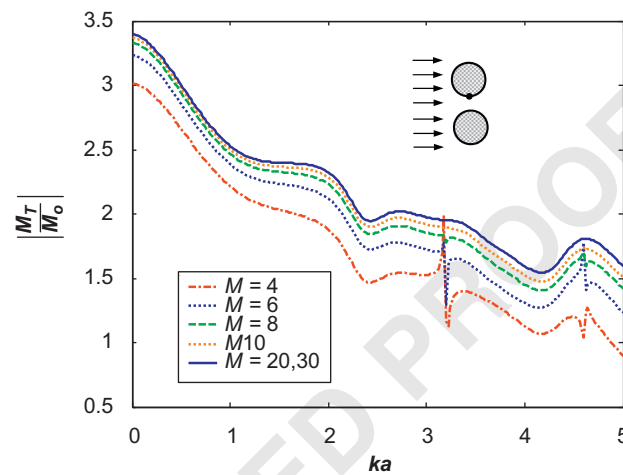


Fig. 13. DMCF on the upper circular boundary ($\gamma = -\pi/2$) versus the dimensionless wave number by using different number of terms of Fourier series ($L/a = 2.1$).

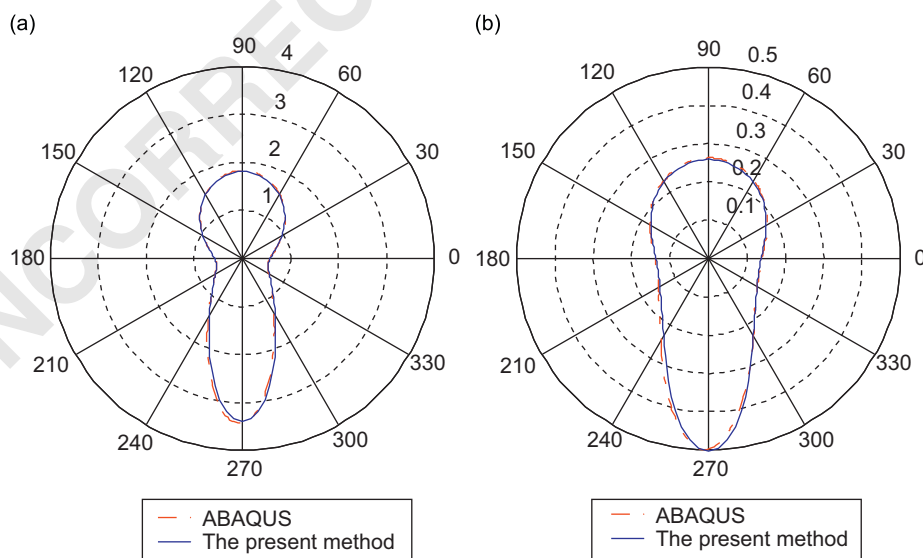


Fig. 14. Distribution of dynamic moment concentration factors on the upper circular boundary of the matrix and inclusion by using the present method and FEM ($L/a = 2.1$)

Please cite this article as: W.M. Lee, & J.T. Chen, Scattering of flexural wave in a thin plate with multiple circular inclusions by using the null-field integral..., *Journal of Sound and Vibration* (2009), doi:10.1016/j.jsv.2009.10.017

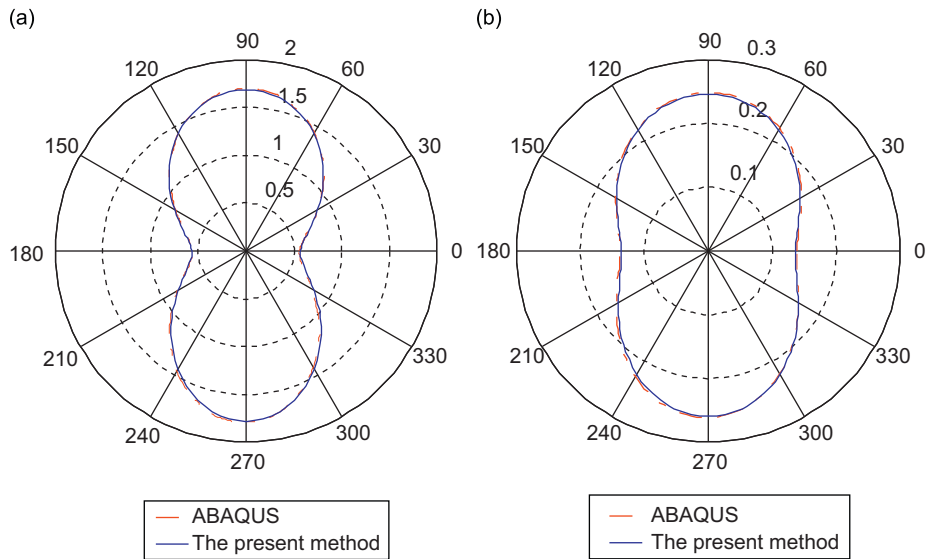


Fig. 15. Distribution of dynamic moment concentration factors on the upper circular boundary of the matrix and inclusion by using the present method and FEM($L/a=4.0$).

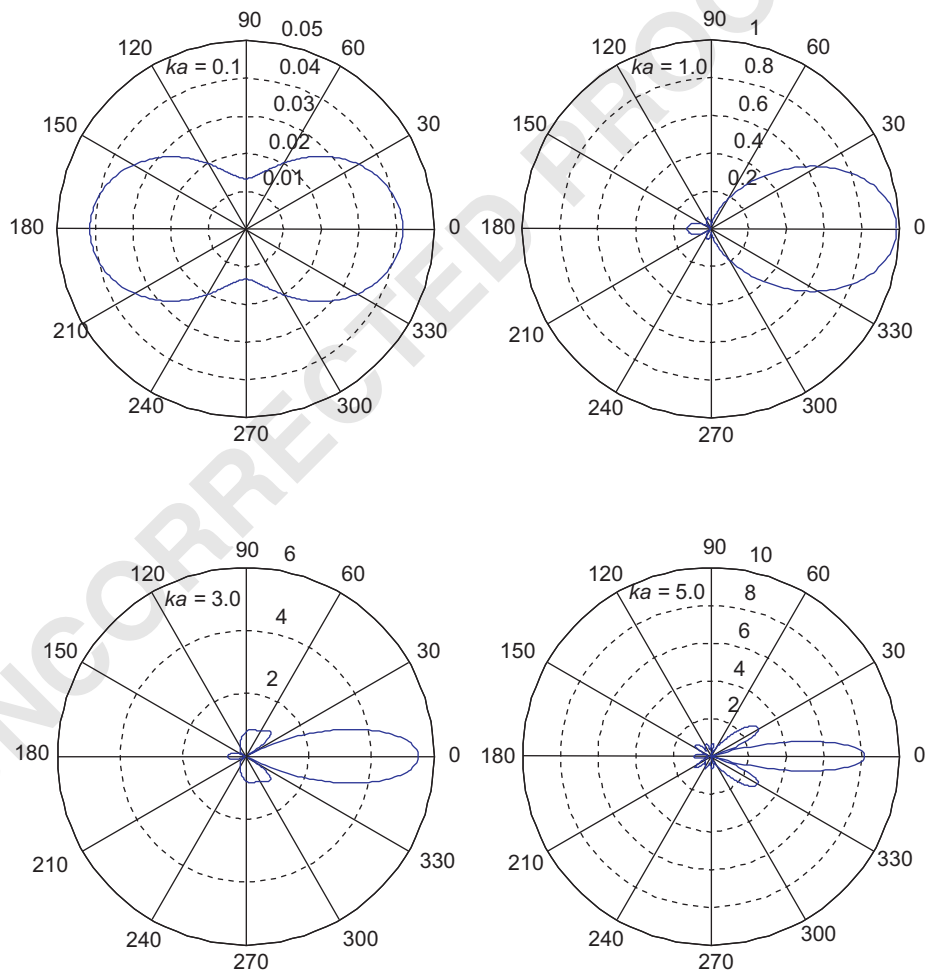


Fig. 16. Far-field scattering pattern for two flexible inclusions with $h_1=h/2$ and $L/a=2.1$ at dimensionless wave numbers $ka=0.1, 1.0, 3.0$ and 5.0

same plate problem is independently solved by using FEM (the ABAQUS software) for comparison. In all cases, the thickness of plate is 0.002 m unless otherwise specified. The general-purpose triangular shell element, S3, of ABAQUS was used to model the plate element. According to theoretical manual of ABAQUS [14], these elements do not suffer from transverse shear locking even though the thickness of the plate is merely 0.002 m.

6.1. Case 1: An infinite plate with uncoated circular inclusions [6]

An infinite plate with one uncoated circular inclusion of radius a , as shown in Fig. 7, subject to incident flexural wave with $\phi_0 = 0$ was firstly considered. Fig. 8 shows the DMCF on the circular boundary, at $\pi/2$, versus the dimensionless wave number by using different number of terms of Fourier series. It indicates that the required number of terms to convergence increases as the incident wave number becomes larger.

In the limit of zero wave number [1] like $ka=0.005$, the excitation of incident wave is equivalent to the static loading with moment $M_{xx} = M_0$ and $M_{yy} = \nu M_0$ at the four sides. For comparison, a 16 m × 16 m plate containing one uncoated inclusion with radius 1m subject to static bending moments, $M_{xx} = 1.0$ and $M_{yy} = 0.3$ at the four sides was considered in the FEM model where 32138 triangle elements was generated. Figs. 9(a) and (b) show the polar plot of dynamic moment concentration factors on the circular boundary of the matrix and inclusion, respectively, by using the present method and FEM. Good agreements can be observed.

Fig. 10 shows the far-field scattering patterns for a flexible inclusion with $h_1=h/2$ at different dimensionless wave numbers $ka=0.1, 1.0, 3.0$ and 5.0 . As ka increases, the scattering pattern inclines toward forward scattering and the associated scattering amplitude also get increasing. Fig. 11 shows the far-field backscattering amplitude versus the dimensionless wave number by using (a) the present method and (b) the method of Norris et al. [6], where the surrounding plate is steel of thickness 0.025 m, solid line for the rigid inclusion and dash-dot line for the inclusion with thickness 0.0125 m. The rigid inclusion means the clamped boundary condition around the circular boundary. It is observed that the proposed results match well with those reported in [6]. It can be found that the amplitude for the scattering response in the far field is $O(\rho^{-1/2})$ to satisfy the radiation condition.

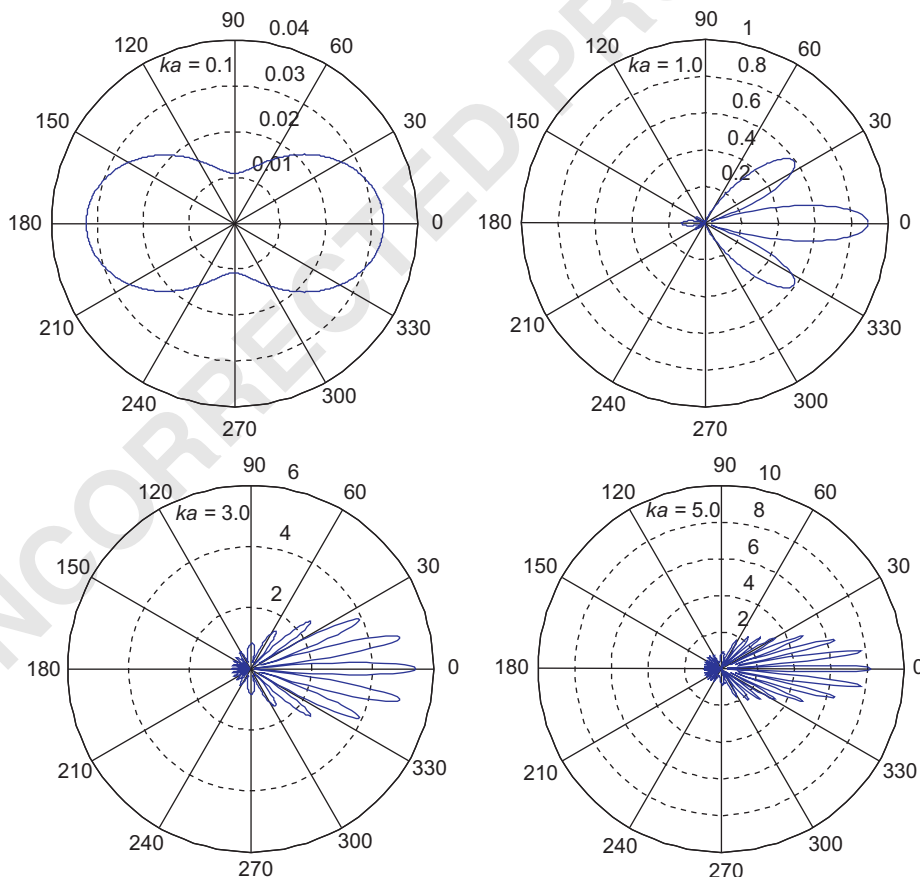


Fig. 17. Far-field scattering pattern for two flexible inclusions with $h_1=h/2$ and $L/a=10.0$ at dimensionless wave numbers $ka=0.1, 1.0, 3.0$ and 5.0 .

To demonstrate the flexural wave scattered by multiple inclusions, two identical uncoated inclusions were considered in Fig. 12, where L is the central distance. In the following simulation, the dimensionless central distance L/a will be used. For $L/a=2.1$, Fig. 13 shows the DMCF on the upper circular boundary of inclusion, at $-\pi/2$, versus the dimensionless wave number by using different number of Fourier series terms. The results using fewer Fourier series terms such as $M=4, 6$ show some peaks at $ka=3.2, 4.6$. They are found to be identical to the true eigenvalues, 3.196, 4.610 [17], of the clamped circular plate with radius equaling to that of the inclusion. Actually they are the so-called fictitious frequencies of the exterior problem. It demonstrates that the increasing number of Fourier series terms can suppress the appearance of fictitious frequencies.

For the dimensionless central distance $L/a=2.1$, Fig. 14 shows the distribution of DMCF on the upper circular boundary, including plate and inclusion, by using both the present method and FEM. It indicates that the maximum DMCF is larger than that of one, as shown in Fig. 9, due to the narrow space between two inclusions. When the space between two inclusions increases such as $L/a=4.0$, the maximum DMCF decreases as shown in Fig. 15. Figs. 16 and 17 show the far-field scattering patterns for two flexible inclusions with $h_1=h/2$ and $L/a=2.1, 10.0$, respectively, at $ka=0.1, 1.0, 3.0$ and 5.0 . After comparing with the results of one inclusion presented in Fig. 10, the far-field scattering amplitude of two inclusions is more or less twice as large as that of one. In addition, the associated fluctuation along the angular direction of two inclusions is more evident than that of only one. Moreover, this trend becomes obvious as the dimensionless central distance increases.

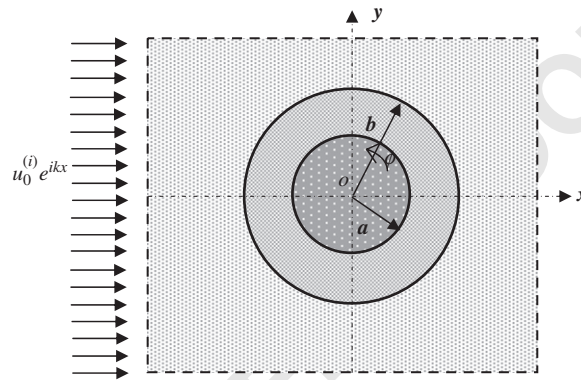


Fig. 18. An infinite plate with a coated inclusion subject to an incident flexural wave.

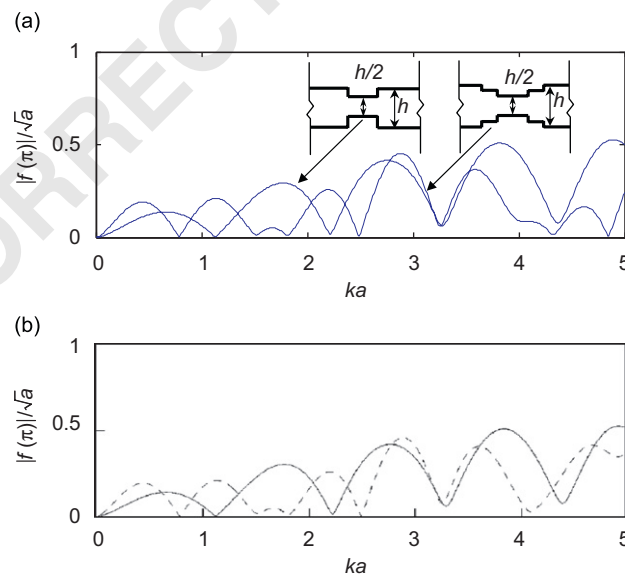


Fig. 19. Far-field backscattering amplitude versus the dimensionless wave number for a plate with an uncoated flexible inclusion with $h_1=h/2$ (solid curve) and an identical inclusion surrounded by a coating with $h_2=3h/4$ (dashed curve), by using (a) the present method and (b) the method of Norris et al. [6] and Squire et al. [7].

6.2. Case 2: An infinite plate with coated inclusions [7]

An infinite plate containing one coated inclusion with inner and outer radius of a and b , respectively, subject to the incident flexural wave with $\phi_0 = 0$ was considered in Fig. 18. Comparing with uncoated inclusion, convergence study indicates that the rate of convergence decreases and the required number of terms to convergence increases due to the complicated configuration of the coated inclusion. However, the proposed quasi-static results still agree well with static data by using FEM.

An infinite plate with (1) an unstepped and stepped indentation, and (2) an unstepped and stepped protrusion, subject to the incident flexural wave with $\phi_0 = 0$ was considered in [7]. Figs. 19 and 20 show the far-field backscattering amplitude versus the dimensionless wave number for indentation and protrusion by using (a) the present method and (b) the method of Norris et al. [6] and Squire et al. [7], respectively. It is indicated that the proposed results match well with those of Norris and Vemula [6] for uncoated inclusion and agree with those of Squire [7] for the coated inclusion except at larger wave number. It shows that, for unstepped cases, the far-field backscattering amplitude of indentation increases with the wave number increasing but that of protrusion decreases. For stepped cases, the far-field backscattering amplitudes are more complicated and the number of troughs increases.

In the end, we consider two coated inclusions subject to the incident flexural wave with $\phi_0 = 0$ as shown in Fig. 21. For $L/a=4.1$, Fig. 22 shows the convergence analysis for the upper circular boundary of annular inclusion, at $-\pi/2$ and some peaks appear at $ka=1.6, 2.3$ due to using fewer Fourier series terms. They are found to be equal to the true eigenvalues, 1.5980, 2.3060 [17], of the clamped circular plate with radius equaling to the outer radius of coated inclusion. Figs. 23

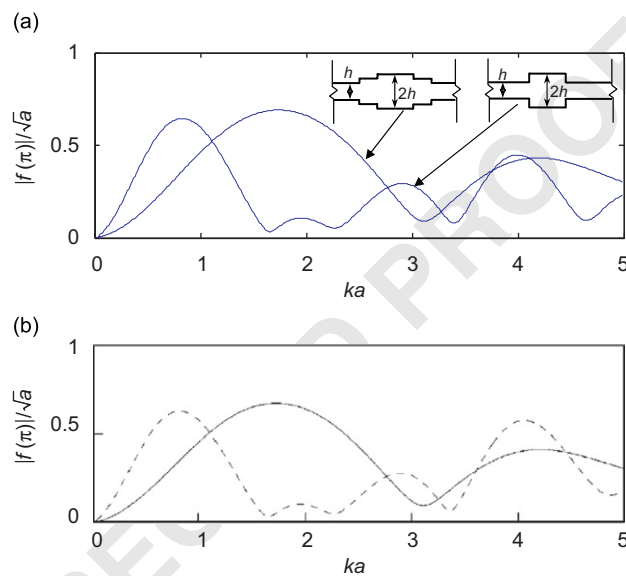


Fig. 20. Far-field backscattering amplitude versus the dimensionless wave number for a plate with an uncoated flexible inclusion with $h_1=2h$ (solid curve) and an identical inclusion surrounded by a coating with $h_2=1.5h$ (dashed curve) by using (a) the present method and (b) the method of Norris et al. [6] and Squire et al. [7].

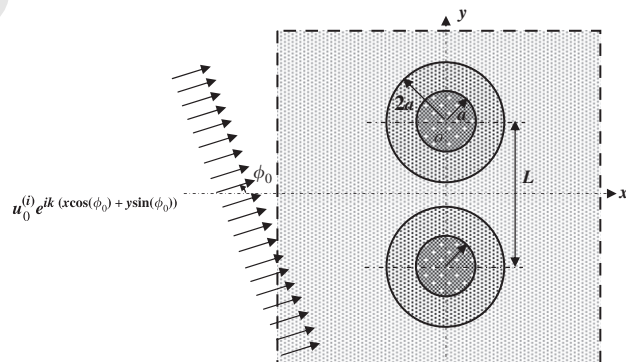
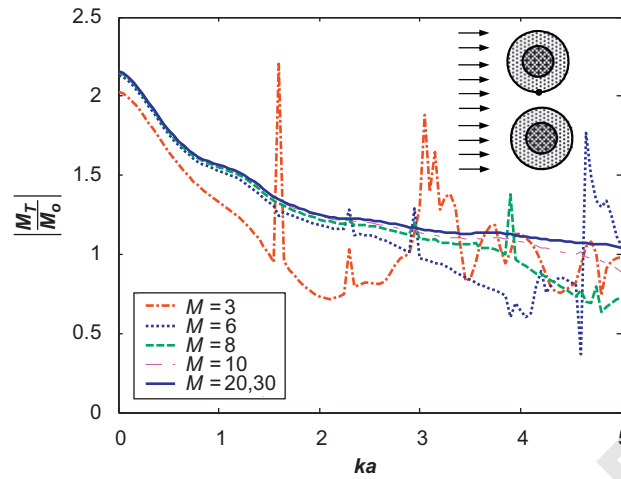
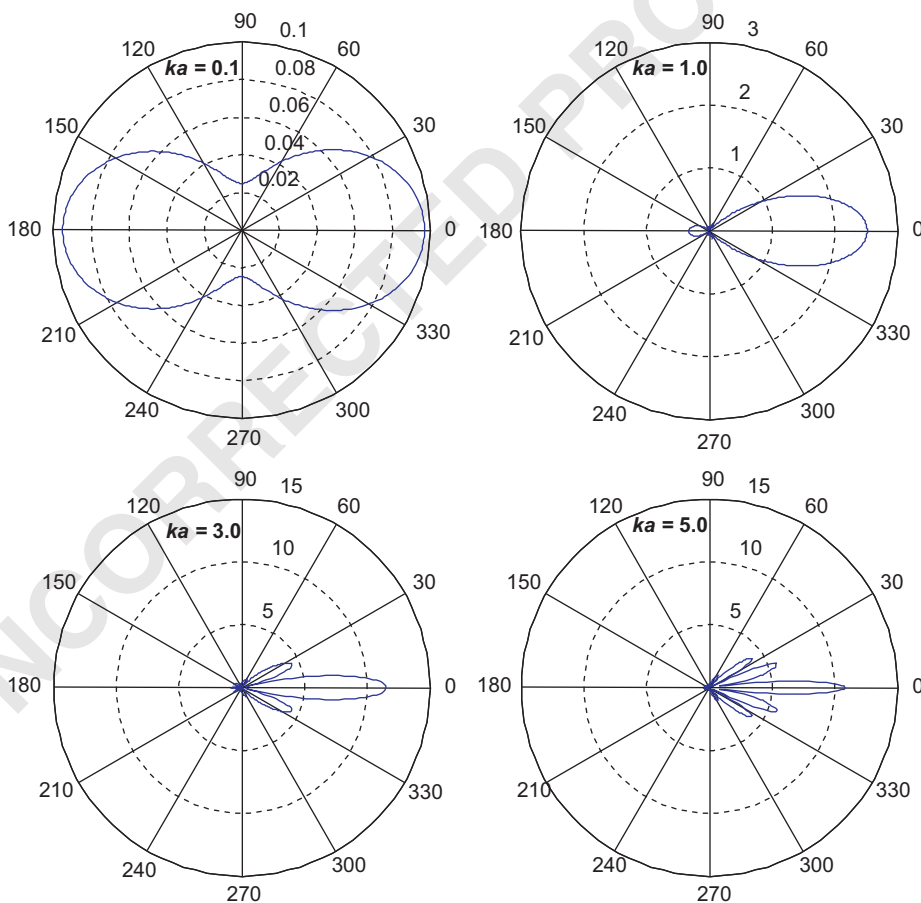


Fig. 21. An infinite plate with two coated inclusions subject to an incident flexural wave.

1 and 24 show the far-field scattering pattern for two flexible inclusions with $h_1=h/2$ and $L/a=4.1, 20.0$, respectively,
 3 surrounded by a coating of twice the radius with $h_2=3h/4$ at different dimensionless wave numbers $ka=0.1, 1.0, 3.0$ and 5.0 .
 5 After comparing with the uncoated case shown in Figs. 16 and 17, the fluctuation of far-field scattering along the angular
 7 direction is more evident, especially at high wave number.



9
11
13
15
17
19
21
23
25
Fig. 22. DMCF on the upper circular boundary ($\theta=-\pi/2$) versus the dimensionless wave number by using different number of terms of Fourier series ($L/a=4.1$).



27
29
31
33
35
37
39
41
43
45
47
49
51
53
55
57
59
61
Fig. 23. Far-field scattering pattern for two flexible inclusions with $L/a=4.1$, $h_1=h/2$, surrounded by a coating of twice the radius with $h_2=3h/4$ at dimensionless wave numbers $ka=0.1, 1.0, 3.0$ and 5.0 .

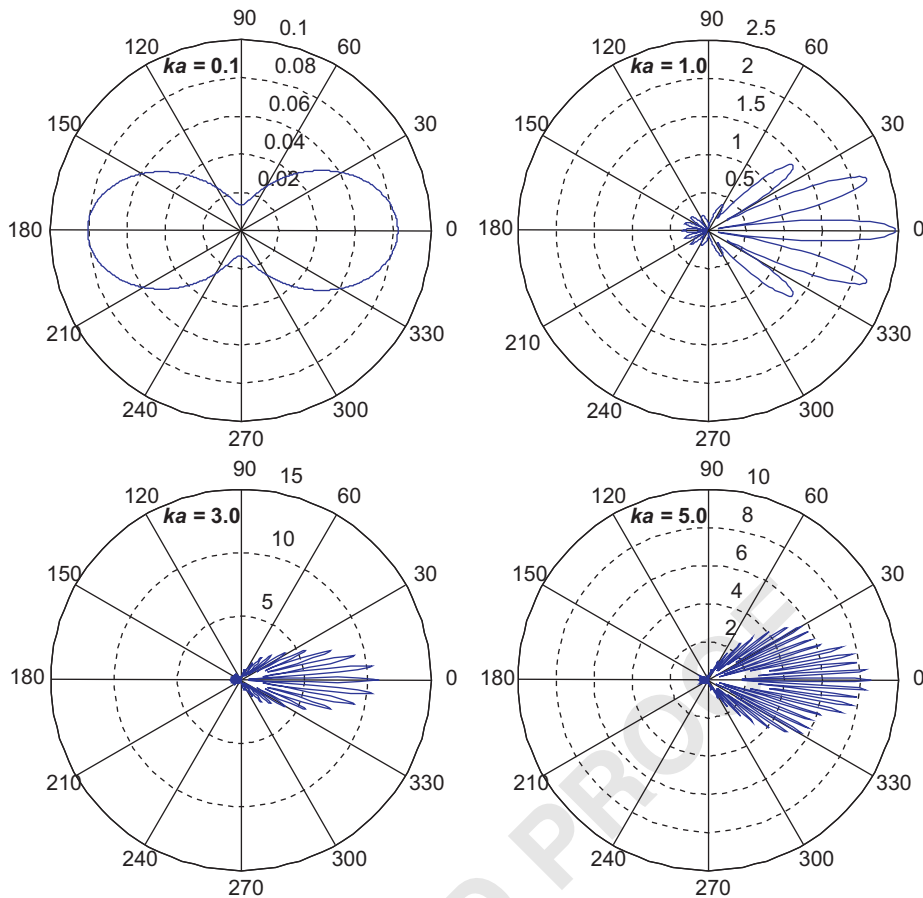


Fig. 24. Far-field scattering pattern for two flexible inclusions with $L/a=20.0$, $h_1=h/2$, surrounded by a coating of twice the radius with $h_2=3h/4$ at dimensionless wave numbers $ka=0.1, 1.0, 3.0$ and 5.0 .

In summary, the space between scatterers has the different effect on the near-field DMCF and the far-field scattering pattern, respectively. Specifically, the near-field DMCF increases as L/a decreases, as shown in Figs. 14 and 15, but the fluctuation of the far-field scattering along the angular direction becomes evident when L/a increases, as shown in Figs. 16, 17, 23 and 24. It implies that the multiple scattering can be simplified by using the single-scattering approximation in studying the near field problem when the spacing between scatterers is large enough, but the far field study cannot follow this rule.

Our semi-analytical method has advantages over both analytical method and the conventional BEM. First, it is clearly convinced that the null-field integral equation approach is applicable to problems with multiple canonical inclusions which the analytical solution is not available. Second, the Fourier series is employed to represent the boundary density and it can be considered as natural coordinates. Consequently, our semi-analytical method has better accuracy over the conventional BEM. In summary, our proposed method has several advantages of (1) free of principal value (2) fast convergence and high accuracy (3) well-posed model. The only disadvantage is that the application to other shape is limited to the degenerate kernel if it is not provided.

7. Concluding remarks

A semi-analytical approach to solve the problem of flexural wave scattered by multiple circular inclusions in an infinite thin plate was presented. The proposed semi-analytical method has advantages over both the analytical methods and the numerical methods, such as the conventional BEM. On one hand, it is clearly convinced that the null-field integral equation approach is applicable to problems with multiple canonical inclusions which cannot be solved easily by analytical methods. On the other hand, it is supposed that this semi-analytical method should have advantages, such as the better accuracy over the conventional BEM. Our studies focus on the issues of DMCF around the circular inclusion and the far-field scattering pattern. For an infinite plate with one circular inclusion, good agreement between the present method and analytical solution is observed. For the cases of multiple inclusions, the quasi-static results match well with the static results from FEM using ABAQUS. Numerical results indicate that DMCF of two inclusions is apparently larger than that of

one. Moreover it indicates that the space between two inclusions has different effects on the near-field DMCF and the far-field scattering pattern. It is helpful for further study on the multiple scattering. As seen from the numerical results, the proposed method provides a semi-analytical solution for the problem of scattering flexural wave by multiple circular inclusions in an infinite thin plate subject to the incident wave, since its analytical solution is not yet available to date.

References

- [1] Y.H. Pao, C.C. Mow, *Diffraction of Elastic Waves and Dynamics Stress Concentration*, Crane-Russak, New York, 1972.
- [2] G. Nishimura, Y. Jimbo, A dynamical problem of stress concentration, *Journal of the Faculty of Engineering, University of Tokyo, Japan* 24 (1955) 101.
- [3] Y.H. Pao, Dynamical stress concentration in an elastic plate, *Transactions of the ASME Journal of Applied Mechanics* (1962) 299–305.
- [4] D.L. Young, C.C. Tsai, Y.C. Lin, C.S. Chen, The method of fundamental solutions for eigenfrequencies of plate vibrations, *CMC: Computers, Materials, & Continua* 4 (1) (2006) 1–10.
- [5] Y. Leviatan, E.T. Erez, M.J. Beran, A source-model technique for analysis of flexural wave scattering in a heterogeneous thin plate, *The Quarterly Journal of Mechanics and Applied Mathematics* 45 (1992) 499–514.
- [6] A.N. Norris, C. Vemula, Scattering of flexural waves on thin plates, *Journal of Sound and Vibration* 181 (1995) 115–125.
- [7] V.A. Squire, T.W. Dixon, Scattering of flexural waves from a coated cylindrical anomaly in a thin plate, *Journal of Sound and Vibration* 236 (2) (2000) 367–373.
- [8] C.H. Wang, F.K. Chang, Scattering of plate waves by a cylindrical inhomogeneity, *Journal of Sound and Vibration* 282 (2005) 429–451.
- [9] S.Z. Peng, Flexural wave scattering and dynamic stress concentration in a heterogeneous plate with multiple cylindrical patches by acoustical wave propagator technique, *Journal of Sound and Vibration* 286 (2005) 729–743.
- [10] P.A. Martin, *Multiple Scattering Interaction of Time-Harmonic Wave with N Obstacles*, Cambridge University Press, Cambridge, 2006.
- [11] W.M. Lee, J.T. Chen, Null-field integral equation approach for free vibration analysis of circular plates with multiple circular holes, *Computational Mechanics* 42 (2008) 733–747.
- [12] R. Kress, *Linear Integral Equations*, Springer, New York, 1989.
- [13] S. Kobayashi, N. Nishimura, Transient stress analysis of tunnels and caverns of arbitrary shape due to traveling waves, in: P.K. Banerjee, R.P. Shaw (Eds.), *Developments in Boundary Element Methods—II*, Applied Science, London, 1981, pp. 177–210.
- [14] ABAQUS 6.5, *Hibbitt, Karlsson and Sorensen, Inc.*, RI, 2004.
- [15] M. Kitahara, *Boundary Integral Equation Methods in Eigenvalue Problems of Elastodynamics and Thin Plates*, Elsevier, Amsterdam, 1985.
- [16] G.N. Watson, *A Treatise on the Theory of Bessel Functions*, second ed., Cambridge Library edition, Cambridge, 1995.
- [17] A.W. Leissa, *Vibration of plates*, NASA SP-160 (1969).